https://doi.org/10.1016/j.conbuildmat.2023.134387

Influence of high temperatures on the mechanical and microstructural properties of hybrid steel-basalt fibers based ultra-high-performance concrete (UHPC)

Mehran Khan, Jiancong Lao, Muhammad Riaz Ahmad*, Jian-Guo Dai*

Department of Civil and Environmental Engineering, The Hong Kong Polytechnic University, Hung Hom, Kowloon, Hong Kong, China

Corresponding author: mriaz.ahmad@polyu.edu.hk; cejgdai@polyu.edu.hk

Influence of high temperatures on the mechanical and microstructural properties of hybrid steel-basalt fibers based ultra-high-performance concrete (UHPC)

Abstract: One of the major problem in ultra-high-performance concrete (UHPC) after exposure to high-temperatures is explosive spalling. Adding a single type of fibers alone is insufficient for suppressing such spalling, and therefore, hybridization of fibers has been adopted, particularly steel with organic fibers. However, the degradation of organic fibers at ambient and elevated temperatures is a significant challenge in the long term and needs to be addressed. Recently, inorganic basalt fibers have been considered as an alternative to organic fibers due to their better mechanical strength and high-temperature resistance characteristics. In this study, hybridizing steel with basalt fiber is proposed as a potential solution to the aforementioned problem. The spalling behavior, residual compressive strength, microstructure, porosity, hydration kinetics, phase decomposition, and quantification of hydration products were evaluated for hybrid steel-basalt fiber reinforced UHPC after exposure to high-temperatures. The study results indicated that hybrid steel-basalt fiber reinforced UHPC successfully prevented explosive spalling behavior. The use of inorganic mineral basalt fibers offers a promising solution for developing UHPC with superior high-temperature resistance.

Keywords: Ultra-high-performance concrete, basalt fibers, explosive spalling, elevated temperatures, compressive strength.

1. Introduction

In recent years, Ultra-high-performance concrete (UHPC) has gained popularity as a promising construction material globally due to its superior mechanical characteristics and excellent durability [1-4]. UHPC typically exhibits high compressive strength ($\geqslant$ 120 MPa), low

permeability, and a dense microstructure due to its high particle packing density and low water-to-binder (w/b) ratio [5-7]. However, the low permeability and compact microstructure of UHPC make it more susceptible to explosive spalling during fire [8-11]. Spalling of UHPC during fire is caused by vapor pressure and thermal induced stress [12, 13]. At elevated temperatures, the migration and escape of water vapor inside UHPC are restricted due to its highly packed microstructure [12, 14]. At the same time, thermal induced stress causes thermal cracking, ultimately leading to strength degradation of UHPC. Therefore, it is crucial to avoid the problem of explosive spalling in UHPC to ensure the safety of UHPC structures during fire.

To prevent spalling in UHPC, the commonly used method is to incorporate steel fibers, polymer fibers, and natural fibers [15-17]. However, steel fiber alone is not effective to avoid the explosive spalling of UHPC [14, 18, 19]. Thus, the effective way to avoid the explosive spalling of UHPC is using hybridization of steel fiber with polymer fiber and/or natural fiber as compared to that of single fiber reinforced UHPC [8, 12, 14, 20-23]. The natural fibers are promising alternative to polymer fibers in UHPC and gains the significant attention in construction industry considering the cradle-to-cradle concept on usage of sustainability concept [19, 22]. It was found that hybrid of steel/polymer fiber together with natural fiber (sisal, jute, and flax) have a great potential to avoid the spalling of UHPC at elevated temperature [12, 14, 19]. However, these studies focused on the combined use of steel fiber with organic plant fiber (sisal, jute, and flax) in UHPC at elevated temperature and these organic plant fibers decomposed at a temperature around 400°C and do not contribute to the strength. The degradation of natural fibers is still a challenge to solve especially at elevated temperatures and in long term due to their biodegradable nature. The information related to high-temperature resistance of inorganic natural mineral fiber in UHPC is

still limited especially the hybridization of steel with inorganic mineral fiber (Basalt fiber having high-temperature resistance) is rarely investigated.

Basalt fiber (BF) is a type of high-temperature resistance inorganic natural mineral fiber with excellent mechanical strength [24-28]. It is also environmentally safe, non-toxic, and cost-effective, obtained by melting basalt rocks at 1400°C [29, 30]. Compared to other fibers such as carbon, basalt fiber is cheaper, and has lower embodied energy and manufacturing costs. Furthermore, its fabrication process does not involve any additives that harm the environment [31-34]. The use of inorganic mineral basalt fibers has become increasingly important in the manufacturing of UHPC at ambient temperature [35-37] as it shows great potential as an alternative to other organic (jute, flax, and sisal) fibers due to its excellent mechanical strength, high-temperature resistance, environmental safety, and cost-effectiveness. Therefore, it is worth exploring the behavior of basalt fibers and steel fibers in UHPC to prevent spalling and ensure the safety of UHPC structures during fire.

The specific objectives of this research are: (1) to identify the role of hybrid steel-basalt fiber in preventing spalling behavior of UHPC after exposure to high-temperatures, (2) to evaluate the residual compressive strength of hybrid steel-basalt fiber reinforced UHPC after exposure to high-temperatures, (3) to examine the microstructure of hybrid steel-basalt fiber reinforced UHPC after exposure to high-temperatures, (4) to analyze the effect of high-temperature on the porosity of hybrid steel-basalt fiber reinforced UHPC and (5) to examine the hydration kinetics, phase decomposition, and quantification of hydration products for basalt fiber-UHPC based system after exposure to high-temperatures. Various techniques were used, including isothermal calorimetry, thermo-gravimetric analysis, Fourier transform infrared analysis, compressive strength tests, microstructure observations, and micro-focus X-ray computed tomography analysis. The

knowledge obtained from the current study will serve as the foundation for developing an efficient hybrid fiber reinforced UHPC that can withstand elevated temperatures and resist explosive spalling. This will ultimately ensure the safety of UHPC structures that are exposed to extreme fire events.

2. Experimental Details

2.1.Raw materials

The raw materials used for preparation of UHPC include OPC, silica fume, fly ash, sand, superplasticizer, steel fiber and basalt fiber. OPC (Type I 52.5 N) was supplied by Green Island Cement Company Limited (Hong Kong). Silica fume was acquired from Shandong Boken Silicon Materials Company Limited (China). Class F fly ash as per the ASTM C618-19 [38] was provided by CLP Power HK Ltd. Table 1 shows the chemical composition of OPC, silica fume and fly ash obtained by XRF spectroscopy. The main elements in OPC were SiO_2 (18.6%) and CaO (66.7%). The fly ash was mostly comprised of Al_2O_3 (26%) and SiO_2 (47.7%), and silica fume mostly contained SiO_2 (96.1%). The particle size distribution curves obtained by the Laser diffraction technique for OPC, silica fume, fly ash, and silica sand are shown in Fig 1. The maximum particle sizes of OPC, silica fume, fly ash were less than 100 μm, whereas the mean particle size of silica sand was less than 300 μm. The XRD patterns of the raw materials are shown in Fig 2. The primary phases in OPC were alite, and belite, while the silica fume mainly consisted of amorphous phases (as shown by a visible broad hump from 15-35° 2θ) along with quartz. The primary phases of fly ash were crystalline quartz, mullite and amorphous phases (hump around 15-35° 2θ). In addition, the polycarboxylate ether based superplasticizer (SP) was used as the water reducer. Furthermore, steel fiber and basalt fiber were used as the reinforcement in UHPC. The steel fibers with a length

of 13 mm and diameter of 200 μm were used as shown in Fig 3(a), whereas the basalt fibers with a length of 12 mm and diameter of 20 μm were used as shown in Fig 3(b).

Table 1. Chemical composition of OPC, silica fume and fly ash (%)

Materials	CaO	SiO_2	SO_3	Al_2O_3	K_2O	MgO	Fe_2O_3	Others
OPC	66.70	18.60	3.98	5.61	0.71	0.69	3.16	0.55
Silica Fume	0.86	96.10	0.16	0.24	0.79	1.41	0.08	0.38
Fly Ash	6.38	47.70	1.41	26.00	2.10	2.64	11.20	2.57

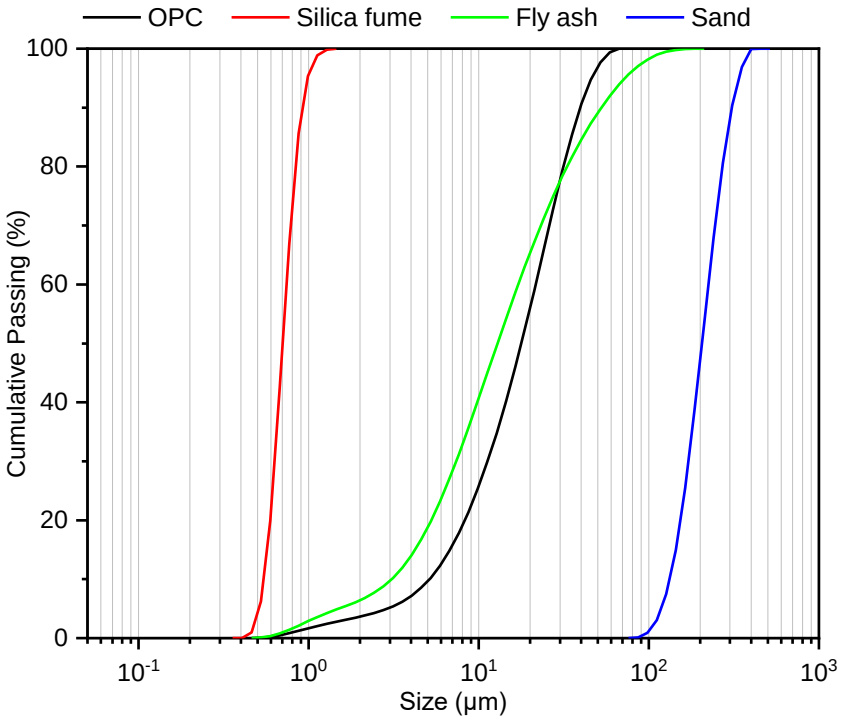

Fig 1. Particle size distribution curve of OPC, silica fume, fly ash and sand

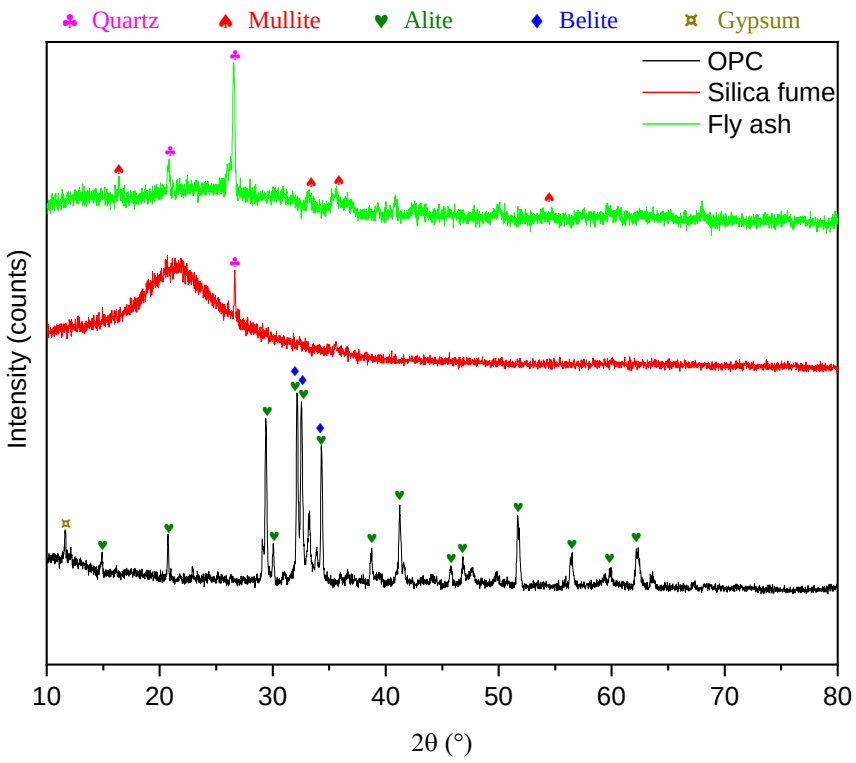

Fig 2. XRD pattern of OPC, silica fume and fly ash

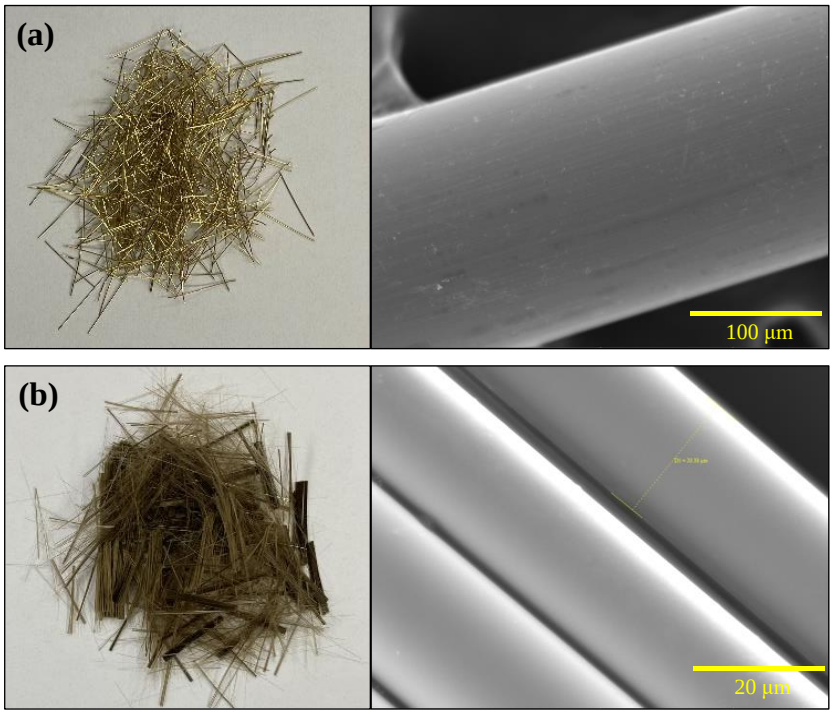

Fig 3. Macro and micro images of fibers: (a) Steel fibers; and (b) basalt fibers

2.2.Specimen preparation

The mix proportions of designed UHPC mixes with fibers contents are shown in Table 2. The mix proportions of all the UHPC mixes are same with fixed raw materials ratio having water (including superplasticizer) to binder ratio of 0.206. It is well known that steel fibers alone are not effective in avoiding the explosive spalling of UHPC even with 2% fiber content [14, 18, 19]. Therefore, hybridization of steel and basalt fiber are considered in this study with total fiber content of 2% to identify the effectiveness of hybrid fibers in UHPC for providing the spalling resistance after exposure to high-temperatures. Fig 4 shows the mixing procedure of UHPC with hybrid fibers and adopted steps are as follows. Firstly, all the raw materials (OPC, sand, silica fume and fly ash) are dry mixed for three minutes followed by addition of basalt fibers with continuous stirring for one more minute. Afterwards, water and superplasticizer were added and further mixed for six minutes. Then, steel fibers were added and continuously mixed for further three minutes. Lastly, the fresh mix was obtained and cast into the moulds. The moulds were covered with a plastic sheet and stored at the ambient air condition. After 24 h, the samples were demoulded and kept for 28 days curing at room temperature (20-25°C).

Table 2. Mix ratio of all UHPC mixes

Matrix	OPC	Silica fume	Fly ash	Silica Sand	Water*/ binder ratio	Steel fiber (vol. %)	Basalt fiber (vol. %)	Total fiber (vol. %)
U	1	0.25	0.25	1.1	0.206	-	-	-
U-2ST	1	0.25	0.25	1.1	0.206	2	-	2
U-1.5ST+0.5BF	1	0.25	0.25	1.1	0.206	1.5	0.5	2
U-1ST+1BF	1	0.25	0.25	1.1	0.206	1.0	1.0	2

Whereas U denotes UHPC; ST denotes steel fiber; and BF denotes basalt fiber. Water = Water + Superplasticizer*

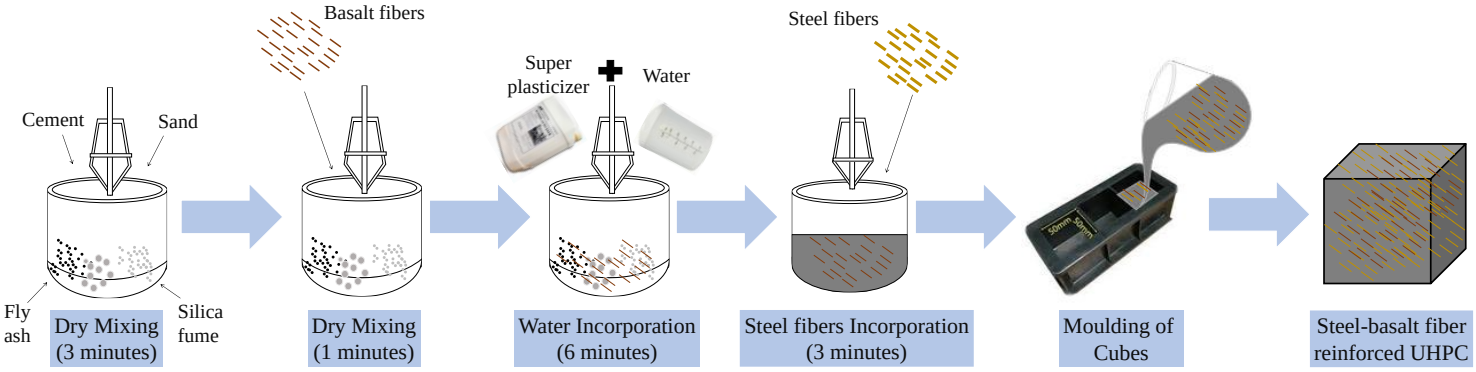

Fig 4. Mixing procedure for hybrid steel-basalt fiber reinforced UHPC

2.3.Heating method

A drying treatment was performed on the UHPC samples before heating as reported in previous studies [39, 40]. The UHPC samples were dried into the oven at 80 °C for 24 hours. After drying treatment, the samples were kept inside a steel cage in an electric furnace (NWTX-13F model supplied by Luoyang Naweite Furnace Co. Ltd, China) with a maximum temperature limit of 1300°C. The severity of spalling is influenced by the heating rate. However, it was reported that when spalling occurs, it consistently happens within a certain range of temperatures, irrespective of the rate at which heating is applied [41]. Some studies [42, 43] used a constant heating rate of 4°C/min according to the standards ASTM E831 [35] to make the heating procedure simple. Whereas a constant heating rate of 2°C/min was reported in other studies [8, 39, 44]. However, the range for heating samples for UHPC was found to be between 2-4°C/min in the literature. In some studies [45-47], the heating rate of UHPC was deliberately set at a low value of 3 °C/min at target temperatures (250 °C, 500 °C, 750 °C and 1000 °C), to minimize the temperature gradient inside and outside of the specimen and ensure complete evaporation of internal water during the initial heating phase. Thus, all the samples were continuously heated at a rate of 3°C/min up to the target temperatures (i.e., 250°C, 500°C, 750°C and 1000 °C). The samples were further kept in furnace

at target temperature for 2 hours to ensure uniform distribution of temperature and then cooled down to normal temperature in furnace.

2.4. Testing procedures

2.4.1. Isothermal calorimetry test

The hydration kinetics was assessed through isothermal calorimetry tests, which were performed with the Calmetrix® I-Cal 4000 instrument. To conduct the tests, around 60 grams of fresh mixture was placed in a plastic vial and monitored for hydration heat over a period of 72 hours. The resulting data was normalized using the weight of the binder. The test measurements were performed three times on each mixture of UHPC containing basalt fiber (0.5% vol.) to ensure accuracy.

2.4.2. Thermogravimetric (TG) analysis

To identify the phase decomposition, thermogravimetric analysis was conducted using the Rigaku Thermo Plus EVO2 equipment. Samples, weighing approximately 10 mg, were heated at a rate of 5°C/min in an argon gas environment from 30°C to 1000°C. The size of samples varies depending on different instruments and the size of the aluminum crucible used. The recommended sample size for analysis is typically around 6-10 mg [48], and most studies in the literature [49, 50] have used UHPC samples of approximately 10 mg for TG analysis.

2.4.3. Fourier-transform infrared analysis

To quantify the hydration products, Fourier-transform infrared analysis was performed using the PerkinElmer UATR-two instrument. The analysis was conducted in transmittance mode at a resolution of 2 cm^{-1} over a wavenumber range of 400-4000 cm^{-1}.

2.4.4. Mechanical properties tests

To assess mechanical properties after exposure to high-temperatures, the compressive strength test was conducted on UHPC samples in compliance with ATSM standard C109/C109M-16 [51]. An average of three specimens were taken for each mix.

2.4.5. Microstructure observations

The microstructure examination was performed within the high vacuum condition using an SEM (Tescan Vega 3 XMU) with a working distance of 18 mm at an accelerating voltage of 20 kV. For evaluating change in appearance of fibers, the steel and basalt fibers were kept into an electric furnace up to the target temperatures of 250°C, 500°C, 750°C and 1000 °C and continuously heated for 2 hours. Later, the surface of fibers was studied using SEM analysis after exposure to high-temperatures. Additionally, the microstructure of plain and hybrid steel-basalt fiber reinforced UHPC samples after exposure to high-temperatures were also studied. After heating, the UHPC specimens were submerged in absolute ethanol for a duration of 7 days to stop the hydration process. Subsequently, the samples were dried in a vacuum oven at a temperature of 40°C for 24 hours.

2.4.6. Porosity test

Finally, the porosity of UHPC samples after exposure to high-temperatures was assessed using the micro-focus X-ray CT system by scanning the specimens with an X-ray tube voltage of 140.0 kV and an X-ray tube current of 40 μA.

3. Results and Discussions

3.1.Influence of elevated temperature on spalling behavior of UHPC

The spalling performance of plain UHPC and hybrid steel-basalt fiber reinforced UHPC after exposure to elevated temperatures is shown in Fig. 5. Spalling of plain UHPC was observed at temperatures of 500°C, 750°C, and 1000°C, resulting in broken specimens in small pieces. Similarly, the spalling of U-2ST was found at temperatures of 500°C, 750°C, and 1000°C, indicating that single fiber incorporation is not effective for avoiding the spalling of UHPC. Moreover, it has been also reported in the literature that steel fiber alone, even with a volume content of 2-3%, was found to be ineffective in preventing the explosive spalling of UHPC [14, 18, 19]. In comparison, no spalling was observed in the hybrid steel-basalt fiber reinforced UHPC from 500°C to 1000°C, demonstrating superior spalling resistance compared to plain UHPC, which is associated with the increased in porosity (will be discussed in section 3.4), facilitated by the addition of fiber due to release of vapor pressure. Therefore, in this study, the hybridization of steel fiber with basalt fiber in UHPC (for a total content of 2%) was found to be effective in providing better spalling resistance with enhanced integrity.

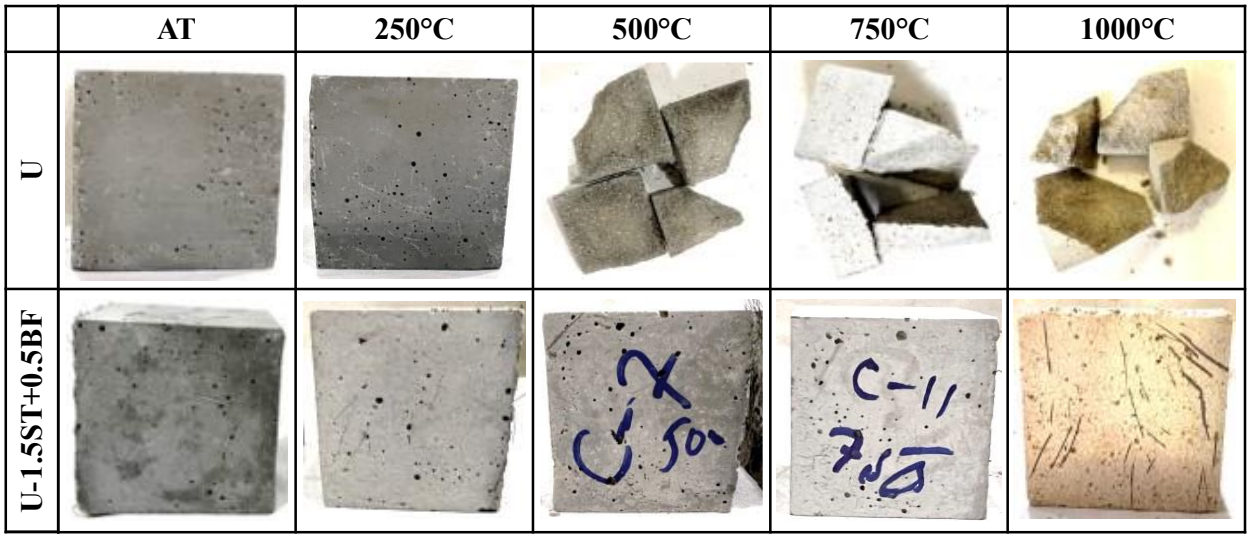

Fig 5. Spalling observation of plain and hybrid steel-basalt fiber reinforced UHPC after exposure to high-temperatures

Fig. 6 displays a closer examination of the cracks formed on the surfaces of the plain UHPC and hybrid steel-basalt fiber reinforced UHPC after exposure to high-temperatures. The crack width and number of cracks gradually increased with a rise in temperature from 250°C-1000°C for both plain UHPC and hybrid steel-basalt fiber reinforced UHPC However, the U-1.5ST+0.5BF and U-1ST+1BF specimens showed better spalling prevention behavior with a lesser crack width and a reduced number of cracks than that of plain and single fiber reinforced UHPC. In contrast, the crack healing and bridging effect of steel and basalt fibers were clearly observed on the surface of the U-1.5ST+0.5BF specimens after exposure to high-temperatures than that of plain UHPC.

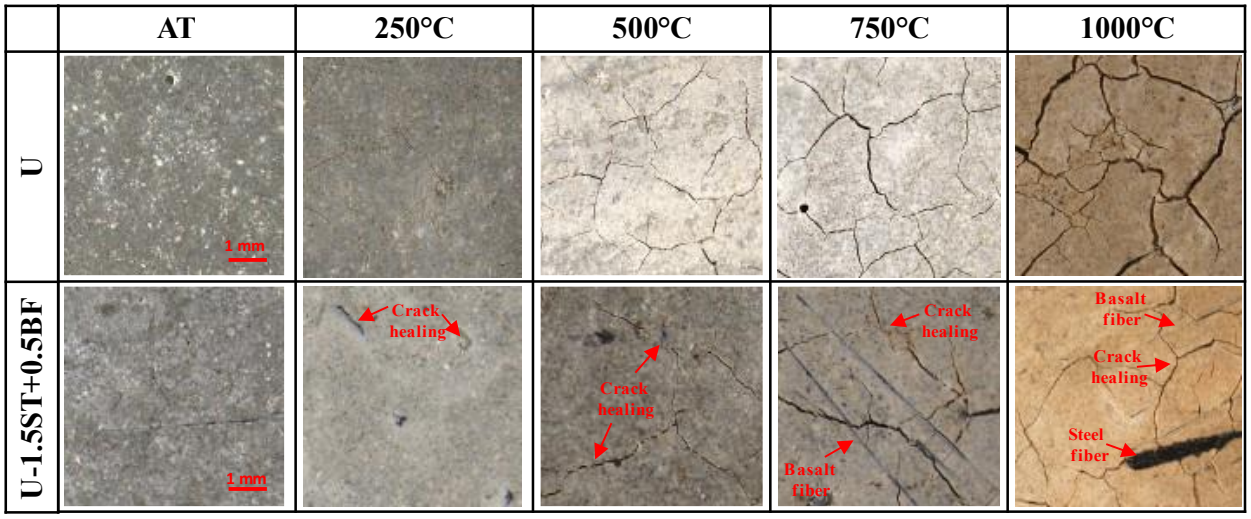

Fig 6. Surface cracking of plain and hybrid steel-basalt fiber reinforced UHPC after exposure to high-temperatures

3.2. Influence of elevated temperature on compressive strength of UHPC

Fig. 7(a) displays the compressive strength, along with the standard deviation, of both plain UHPC and hybrid steel-basalt fiber reinforced UHPC specimens exposed to high temperatures. The standard deviation bars in Fig. 7(a) represent the extent of data dispersion, which remained below 7% for all UHPC specimens at every temperature level. The maximum standard deviation observed for plain UHPC, U-2ST, U-1.5ST+0.5BF, and U-1ST+1BF, across all temperatures, reached values of up to ±1.5 MPa, ±2.1 MPa, ±5.4 MPa, and ±4.1 MPa, respectively. At AT, the compressive strength of plain UHPC, U-2ST, U-1.5ST+0.5BF, and U-1ST+1BF was 126.8 MPa, 147.6 MPa, 135.7 MPa, and 113.4 MPa, respectively. Compared to plain UHPC, the compressive strength of U-1.5ST+0.5BF was increased by 7%, while the compressive strength of U-1ST+1BF was reduced by 10.5%. The addition of 1.5% steel and 0.5% basalt fibers in UHPC resulted in an increased compressive strength due to fiber bridging phenomenon, which provided a positive synergistic effect. However, an increase in basalt fiber content from 0.5% to 1% in UHPC at AT had an inverse effect on compressive strength, causing a noticeable strength reduction. The

increased dosage of basalt fibers from 0.5% to 1.0% results in an increased porosity of UHPC. The incorporation of a higher amount of basalt fibers creates voids that affect the overall density and compactness of UHPC, ultimately leading to a decrease in compressive strength. At 250°C, the compressive strength of plain UHPC, U-2ST, U-1.5ST+0.5BF, and U-1ST+1BF was 140.2 MPa, 159.4 MPa, 145.5 MPa, and 118.3 MPa, respectively. The secondary hydration of the unhydrated clinkers under a high-temperature steam environment in the inner part of the UHPC matrix resulted in increased compressive strength [52-54]. From 500°C to 1000°C, the compressive strength of plain UHPC and U-2ST, could not be determined due to its spalling. However, the compressive strength of U-1.5ST+0.5BF at 500°C, 750°C, and 1000°C was 105.1 MPa, 55.8 MPa, and 35.8 MPa, respectively. No spalling was observed in the steel-basalt fiber reinforced UHPC after exposure to high-temperatures, which indicated a positive synergistic effect by hybrid fibers.

Fig 7(b) demonstrates the normalized compressive strength with respect to AT under elevated temperatures. At 250°C, the compressive strength of U-2ST, U-1.5ST+0.5BF and U-1ST+1BF was increased by 8%, 7% and 4%, respectively. At 500°C, 750°C, and 1000°C, the U-1.5ST+0.5BF could retain 77%, 41% and 26% respectively, of their actual strength at AT. Also, the compressive strength of U-1ST+1BF at 500°C, 750°C, and 1000°C was decreased to 64%, 38% and 21%, respectively, compared to that of AT. Results show that U-1.5ST+0.5BF presented better residual compressive strength than that of U-1ST+1BF, U-2ST, and plain UHPC after exposure to high-temperatures. Thus, the hybrid mix of 1.5% steel and 0.5% basalt fiber content in UHPC was suggested as a better mix for residual compressive strength.

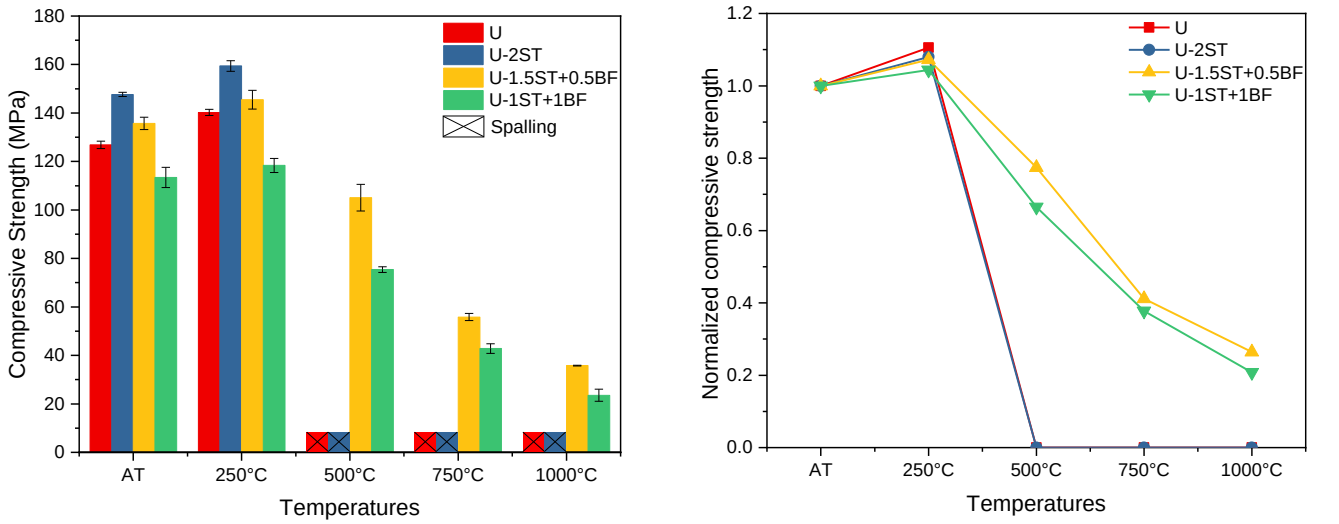

(a) Residual compressive strength (b) Normalized compressive strength with respect to AT

Fig 7. Residual compressive strength of plain and hybrid steel-basalt fiber reinforced UHPC

3.3. Microstructural alterations after exposure to high-temperatures

3.3.1. Morphology of steel fibers after exposure to high-temperatures

Fig 8 shows changes in the appearance of steel fibers with SEM images after exposure to high-temperatures. From ambient temperature (AT) to 250°C, the color of steel fibers was golden, and the surface of the steel fibers did not show any damage, as evidenced by a single fiber SEM image. This shows that the copper-coated surface of the steel fibers had not yet oxidized. At 500°C, the copper coating was oxidized, but the surface of the steel fibers became black. However, the steel fibers were still in good condition and indicated better mechanical properties, as they could be bent at any angle manually by hand, and there was no damage on the fiber surface as evidenced by SEM images. At 750°C, the color of steel fibers became dark black, and oxidation occurred on the surface of the steel fibers as shown in SEM images. Despite this, the steel fibers could still provide some resistance and could be bent manually by hand. At 1000°C, the surface of steel fibers was completely oxidized, and color become silvery grey. At this stage, the steel fibers became brittle and were easy to break without providing any resistance when bent manually by hand.

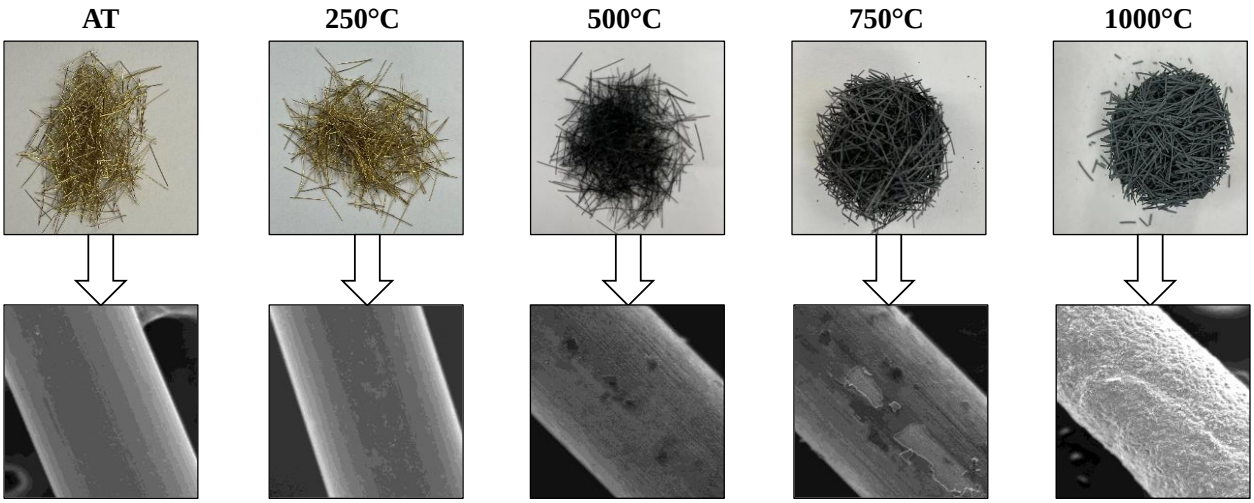

Fig 8. Appearance of steel fibers due to elevated temperature at macroscale (Top) and microscale (bottom)

3.3.2. Morphology of basalt fibers after exposure to high-temperatures

Fig 9 shows the changes in appearance of basalt fibers with SEM images after exposure to high-temperatures. From ambient temperature (AT) to 500°C, the color of basalt fibers remained golden brown, and no changes were observed in their appearance. Additionally, SEM images showed no damage on the surface of basalt fibers after exposure to high-temperatures up to 500°C. At 750°C, the color of basalt fibers turned black, but no damage was observed on their surface. The change in appearance at 750°C was due to the vaporization of the surface treatment agent [55]. At 1000°C, the color of basalt fibers turned dark brown due to further oxidation of metallic elements (Fe^{2+}). At this stage, the basalt fibers were less flexible than at AT but still provided some resistance, and some minor defects appeared on the surface. It is worth mentioning that color changes in appearance of fibers and the oxidation of elements can lead to decreased tensile strength of both steel and basalt fibers after exposure to high-temperatures, as reported in the literature [55].

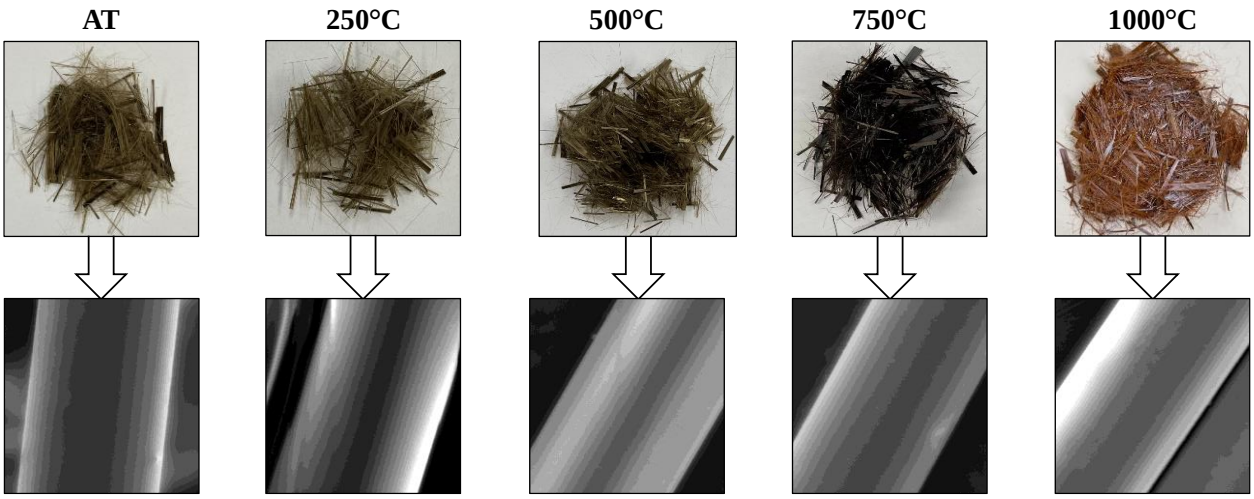

Fig 9. Appearance of basalt fibers due to elevated temperature at macroscale (Top) and microscale (bottom)

3.3.3. Microstructure of plain UHPC after exposure to high-temperatures

The SEM images of plain UHPC after exposure to high-temperatures are presented in Fig 10. At ambient temperature (AT), no instances of cracking were observed in plain UHPC. However, at a temperature of 250°C, cracks were found along the aggregate-matrix interface and in the matrix. The micro cracks observed along the aggregate-matrix interface were caused by thermal incompatibility causing stress in the tangential direction of aggregates, while those micro cracks in the matrix were due to high tensile stress due to water loss-induced shrinkage [56, 57]. Upon exposure to a temperature of 500°C, crack propagation increased in UHPC-OPC, resulting in the emergence of multiple cracks in the radial direction. In addition, the cracks can form when silica sand, specifically quartz (which is a dominant phase of silica aggregate), undergoes a phase transformation from α to β at 573°C [58]. This transformation results in a significant volume expansion, reported in previous studies [59, 60], contributing to a substantial decrease in bonding between the aggregate and the matrix. Furthermore, at a temperature of 1000°C, the cracks became more apparent, leading to a reduction in bonding between the aggregate and matrix. Thus, it was

found that thermal incompatibility between the aggregate and matrix contributes to cracking in plain UHPC after exposure to high-temperatures.

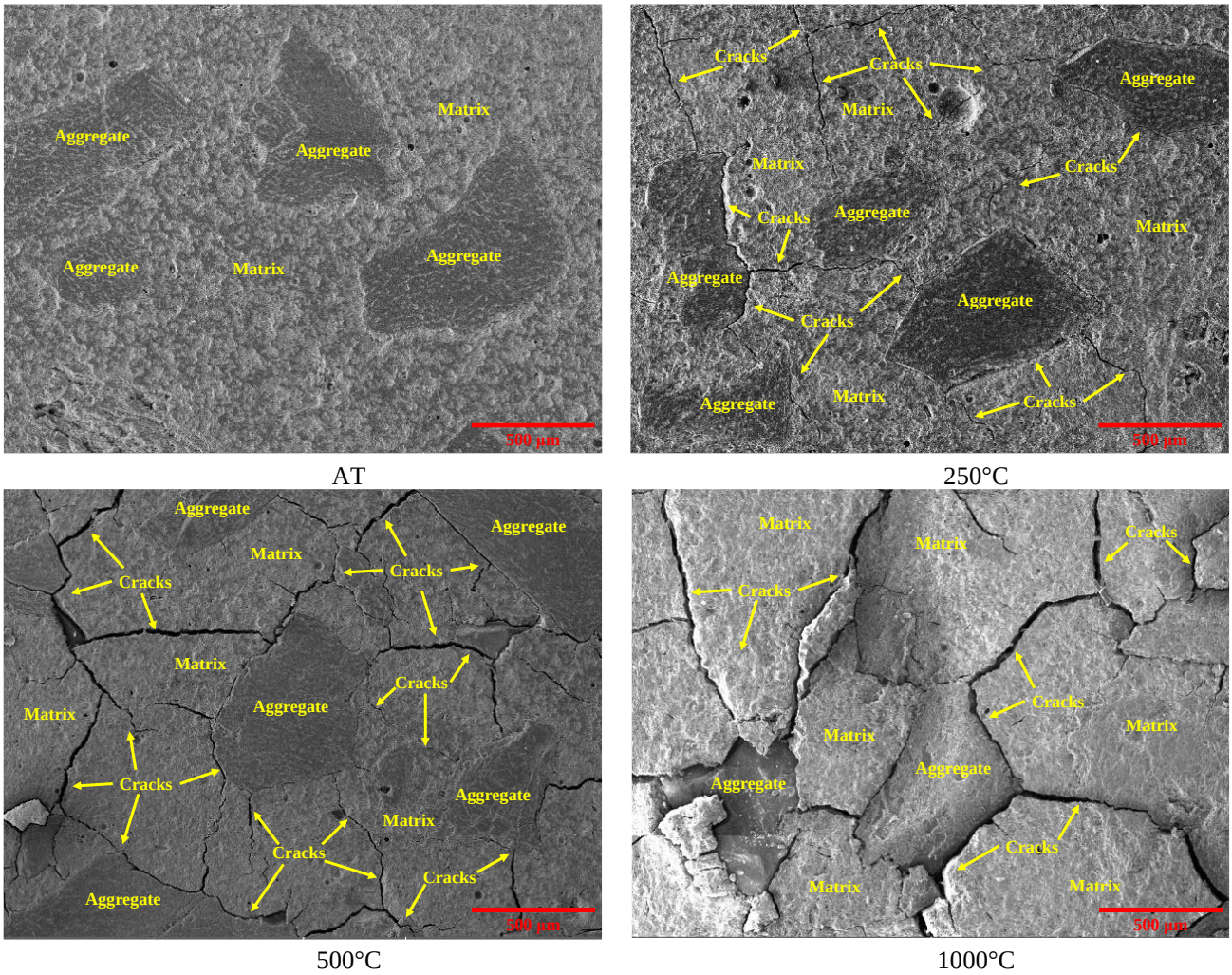

Fig 10. Plain UHPC after exposure to high-temperatures

3.3.4. Microstructure of hybrid steel-basalt fiber reinforced UHPC

The SEM images of hybrid steel-basalt fiber reinforced UHPC (U-1.5ST+0.5BF) after exposure to high-temperatures are presented in Fig 11. At AT, no visible cracks were detected in the hybrid steel-basalt fiber reinforced UHPC. At a temperature of 250°C, cracks were observed along the steel fiber-matrix interface and the aggregate matrix interface. The cracks observed along the steel

fiber-matrix and aggregate-matrix interfaces at a temperature of 250°C are typically due to the thermal incompatibility between the fiber, matrix, and aggregate. However, healed cracks were found at 250°C. The healing of these cracks was attributed to the formation of additional C-S-H gel at higher temperatures. This gel can fill the micro-cracks and voids, effectively healing the cracks. The formation of additional C-S-H gel was evident from the microstructure of the matrix at 250°C, which was observed to be denser and less porous compared to that of AT, indicating the contribution of unreacted particles in the pozzolanic reaction in the presence of water vapor after exposure to high-temperature. This observation suggests that the formation of C-S-H gel was facilitated at 250°C compared to that of AT.

At a temperature of 500°C, the SEM images showed an increased amount of reacted particles in UHPC that make it more porous. This increased amount of pores was attributed to the dehydration of C-S-H gel and the decomposition of $Ca(OH)_2$ [61]. It is notable from the magnified portion of the SEM image that the crack healing through autogenous healing was more effective around the interfaces because these regions provided more reactive surfaces for the reaction products to form and accumulate healing material. These reactions generated new reaction products, such as calcium silicates and aluminates cementitious gel [62], that could fill the cracks up to 60 µm. The addition of hybrid steel-basalt fibers in UHPC reduced the crack width and prevented further propagation of the cracks. On the other hand, the center of the cracks had a larger width, and therefore, the reaction products could not easily accumulate in this region, since it was found that high-temperatures favor faster self-healing process of cracks especially for smaller cracks (< 100 µm) as compared to that of greater cracks [63].

At a temperature of 750°C, the healing of cracks in UHPC was due to the unhydrated/unreacted cement and supplementary cementing particles. The complete healing of cracks was observed at

750°C compared to that at 500°C, resulting in more effective crack healing. Fiber reinforced UHPC had the potential to repair the cracks due to large amount of unhydrated/unreacted cement and supplementary cementing particles after hardening [64, 65]. Silica fume and fly ash are important cementitious materials that play a role in improving the autogenous self-healing behavior of fiber reinforced UHPC [64, 66]. Nonetheless, the partial filling or complete filling of cracks was still beneficial for retaining the mechanical properties of steel-basalt fiber reinforced UHPC after exposure to high-temperatures. However, at a temperature of 750°C, the bond between the steel fibers and the UHPC matrix may weaken due to the oxidation of steel fibers while the basalt fiber still shows good bonding with the UHPC matrix.

At a temperature of 1000°C, crack healing was observed in UHPC due to the transformation of C-S-H gel to $CaSiO_3$ [67, 68]. This transformation process is known as decalcification, which involves the loss of calcium ions from the C-S-H gel and the formation of calcium silicate phases. Decalcification can be accelerated at high-temperatures, leading to the formation of a dense and impermeable layer of $CaSiO_3$ that can fill and seal cracks [69]. At 1000°C, crack healing was observed in hybrid steel-basalt fiber reinforced UHPC, while plain UHPC did not show any healing due to excessive crack propagation as autogenous self-healing process is only observed for smaller cracks (< 100 μm). Overall, the bridging effect of hybrid steel-basalt fiber in UHPC led to better resistance to cracking after exposure to high-temperatures compared to plain UHPC, and the cracks that did occur were partially or completely healed, leading to better mechanical properties of UHPC at high-temperatures. Thus, the addition of basalt fibers creates a network within the UHPC matrix, distributing stresses and controlling crack propagation. Furthermore, basalt fibers can generate voids or pores at high temperatures, serving as waterways for vapor release. This helps alleviate internal pressure and prevents explosive spalling.

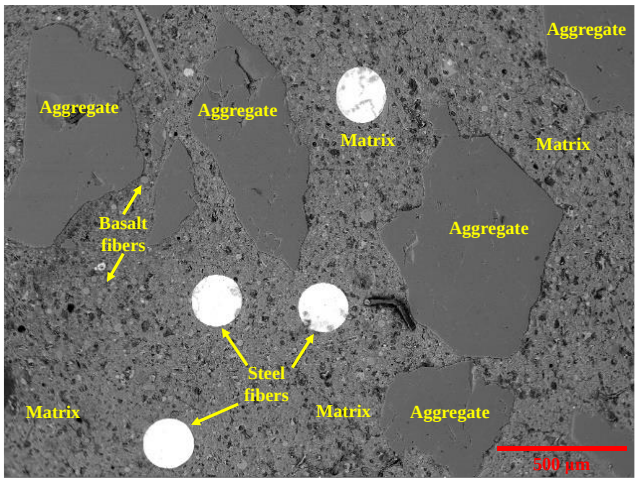

AT

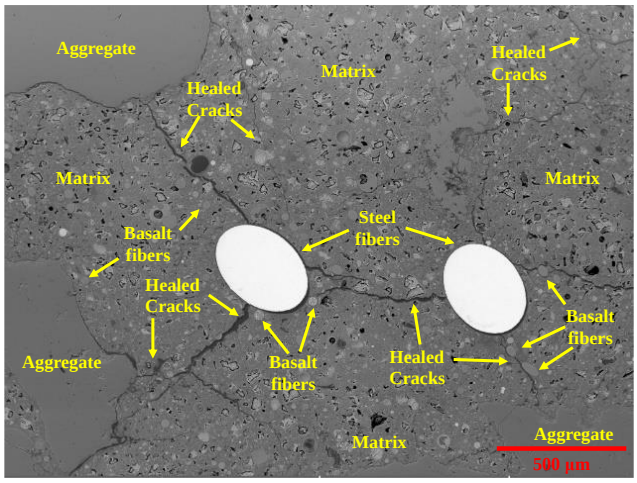

250°C

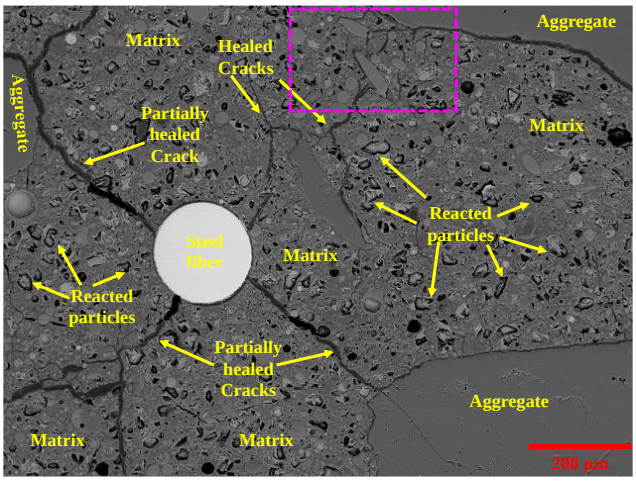

500°C

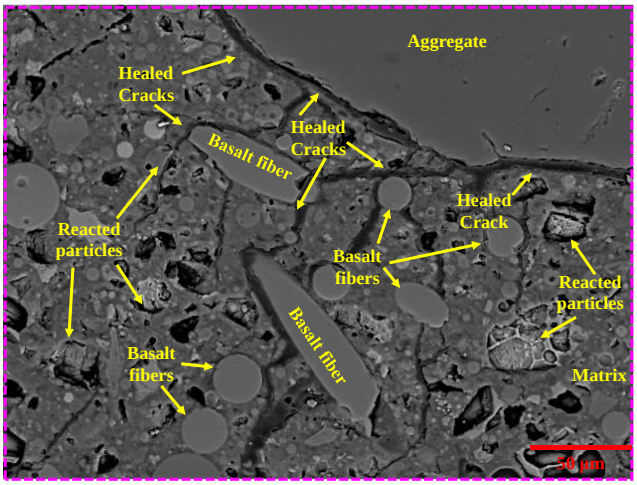

Magnified image of dotted pink area at 500°C

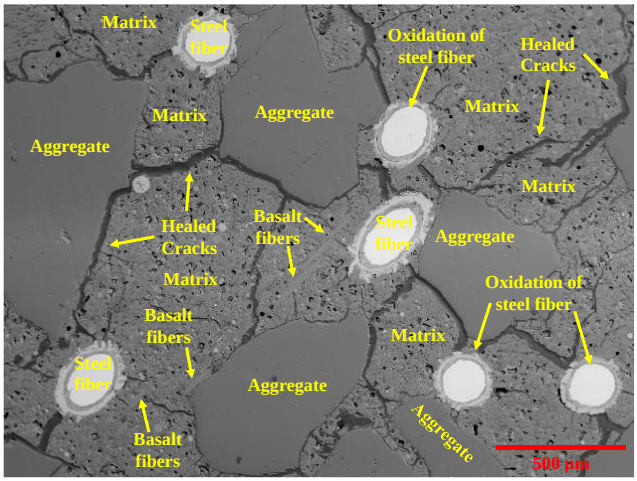

750°C

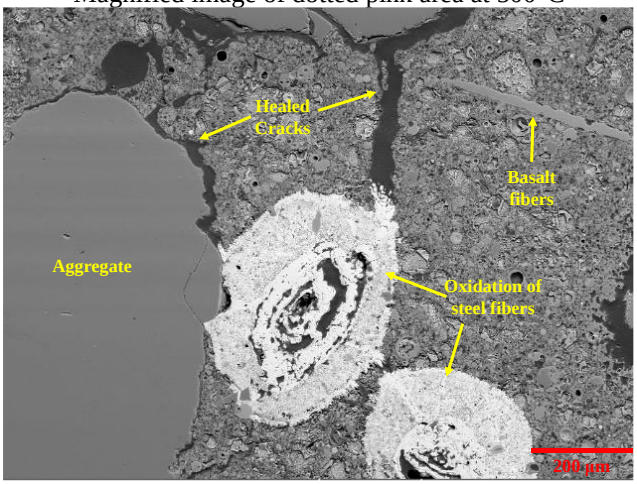

1000°C

Fig 11. Hybrid steel-basalt fiber reinforced UHPC after exposure to high-temperatures

3.4. Porosity of UHPC specimens after exposure to high-temperatures

The Micro XCT test was conducted to assess the porosity of plain and hybrid steel-basalt fiber reinforced UHPC matrix after exposure to high-temperatures, and detailed images of its internal structure are shown in Fig 12. At ambient temperature, the UHPC samples with hybrid fibers (U-1.5ST+0.5BF and U-1ST+1BF) exhibited significantly higher porosity (4.77% and 5.40%, respectively) compared to U-AT (2.07%) as shown in Fig 12(a). However, the porosity of U-1ST+1BF-AT was slightly higher than that of U-1.5ST+0.5BF-AT, indicating that increase in BF content from 0.5% to 1.0% slightly increased the porosity of mixture (refer to Fig 12(c)-(d)). A decline in the porosity of U (from 2.07% to 0.92%) was observed when temperature was increased from ambient temperature to 250°C as shown in Fig (b), indicating a denser matrix at 250°C as evident by SEM in Section 3.6. This decrease in porosity can trap vapors inside the matrix, hindering their release. Conversely, the porosity of U-1.5ST+0.5BF, as shown in Fig (e) also decreased from 4.77% at ambient temperature to 2.57% at 250°C. The comparison of porosity between U-250°C and U-1.5ST+0.5BF-250°C revealed that U-1.5ST+0.5BF-250°C had a higher porosity, which could facilitate the release of vapor pressure after exposure to high-temperatures. However, plain UHPC exhibited explosive spalling at 500°C, so no analysis was carried out for samples between 500°C and 1000°C. In contrast, the hybrid steel-basalt fiber reinforced UHPC displayed an increase in porosity with increasing temperature: 4.29% at 500°C, 6.24% at 750°C, and 10.19% at 1000°C as illustrated in Fig (f)-(h). Compared to that AT, the increase in porosity can be attributed to decomposition of $Ca(OH)_2$ between 400-500°C and C-S-H gel beyond 600°C [61]. The increase in porosity was also observed by SEM in section 3.3.4 and the detailed mechanism of hydration products with microstructural characterization will be explained in next

section 3.5. Compared to the U, the addition of hybrid fibers to UHPC increased its porosity at both ambient and elevated temperatures.

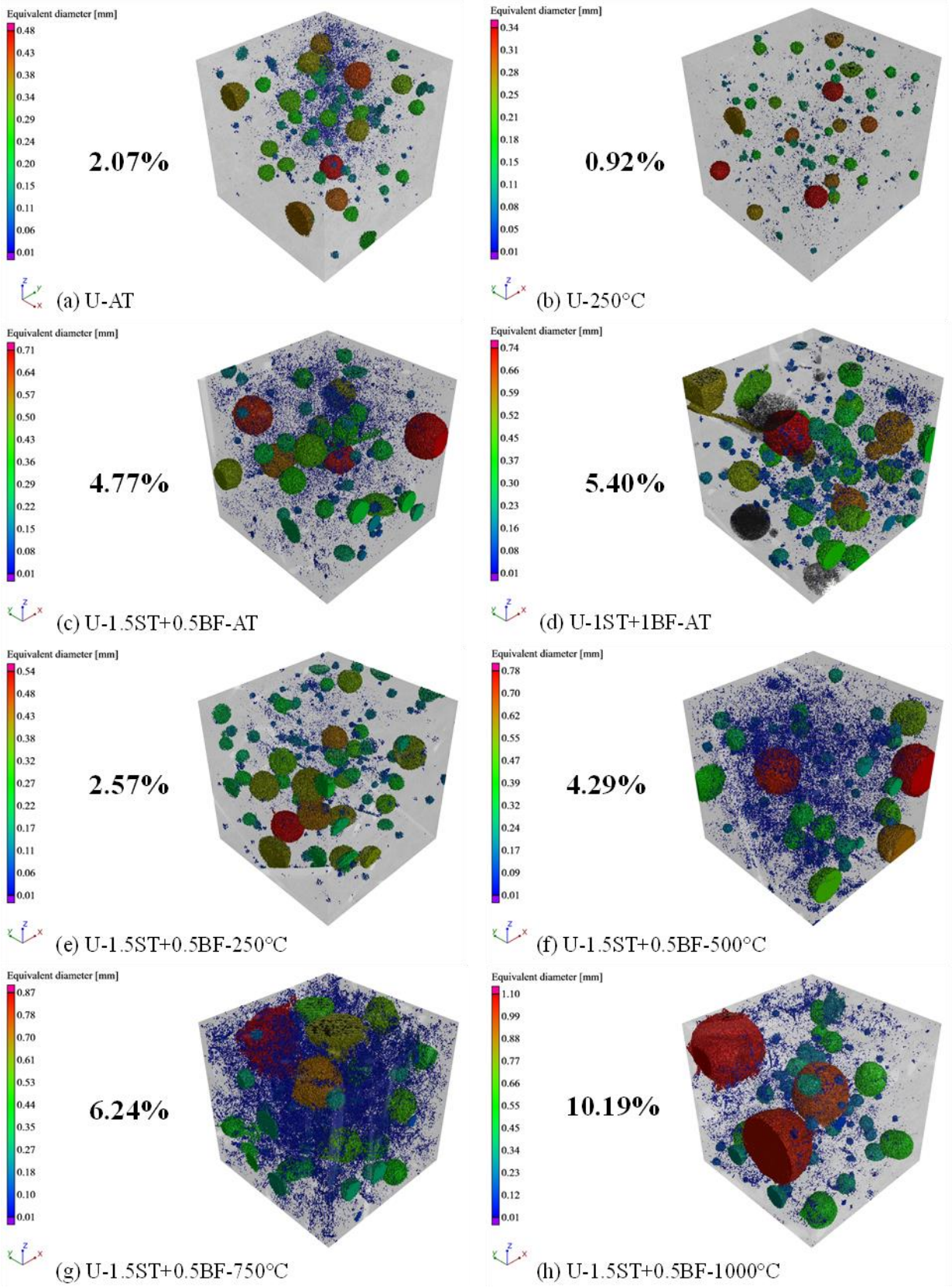

Fig 12. Changes in porosity of plain and steel-fiber reinforced UHPC at different temperatures

3.5. Hydration and microstructure study of plain and fiber reinforced UHPC

Microstructural characterization was performed further to understand the behavior during the physical and chemical processes that occurred during hydration. Steel fiber was not added to the mix primarily for ease of sample preparation (powder form) and to eliminate its influence on the measurement of the hydration reaction of UHPC. This procedure was also reported in the literature [60]. It was reported that basalt fibers were composed of minerals similar to those found in cementitious materials and had a strong chemical bond with the cementitious matrix [36, 70]. Therefore, the hydration kinetics, phase decomposition and quantification of hydration products were performed on basalt fiber reinforced UHPC.

3.5.1. Heat of hydration of plain and fiber reinforced UHPC

The hydration kinetics of basalt fiber used in UHPC was evaluated by calorimetry test. Fig 13(a) shows the rate of heat release during hydration for the first 3 hours, while Fig. 13(b) shows the heat release for 72 hours. Hydration kinetics is a heat-releasing process and usually consists of four periods: the pre-induction period, induction period, acceleration period, and deceleration period [71, 72]. During the pre-induction period (<0.5h), less heat flow was observed in basalt fiber reinforced UHPC binders (U-BF) before the first exothermic peak as compared to plain UHPC (U) binders. Similarly, during the induction period (~0.5h-2h), lower heat flow was found in U-BF than in U. During the acceleration period (~2h-16h), the heat flow of the second exothermic peak was lower for U-BF, however this exothermic peak in U-BF appeared earlier than that of U. This early hydration can be attributed to the addition of basalt fibers, which provides more nucleation sites for the chemical reaction to occur during the acceleration period. The basalt fibers maintain a more uniform distribution of water in U-BF, ultimately promoting the early formation of calcium silicate hydrate (CSH) gel and portlandite ($Ca(OH)_2$). Delannoy, et al. [73]

reported that the increase in the heat flow peak after 4 h is connected to the hydration of alite (C_3S) to CSH phases and precipitation of $Ca(OH)_2$. During the deceleration period (>16h), rate of heat release was lower in U-BF than in U. The cumulative heat of hydration curve, as shown in Fig. 13(a) and Fig. 13(b), clarifies the phenomenon and highlights that U-BF has a lower cumulative heat of hydration than U. This indicates that the basalt fibers act as a thermal insulator, owing to their low thermal conductivity. By adding basalt fibers, the dissipation of generated heat during the hydration process is hindered, resulting in slightly reduced heat flow in U-BF compared to U. As a result, the low heat of hydration due to addition of BF could lead to slightly less formation of CSH gel and $Ca(OH)_2$ compared to U during early stage.

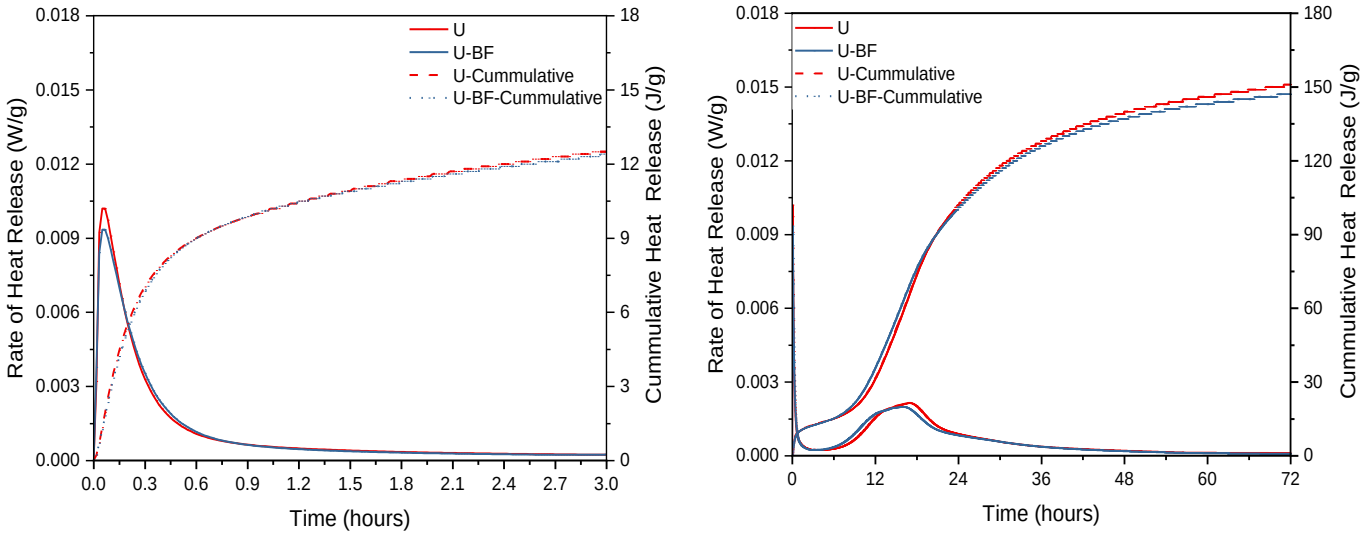

(a) Heat release rate during the first 3 hours (b) Heat release rate up to 72 hours

Fig 13. Heat of hydration for plain and basalt fiber reinforced UHPC

3.5.2. Thermal analysis of plain and fiber reinforced UHPC

The derivative thermogravimetry (DTG) and thermogravimetry (TG) analyses were utilized to investigate the effect of temperature on the hydration products. The DTG curves display four distinct endothermic peaks (Fig 14(a)) of thermal decomposition related to the four stages. In Stage

1 (RT-350°C), the first peak was associated with the dehydration of physically and chemically bound water in ettringite and CSH gel [67, 74, 75]. The lower peak for water loss below 105°C in Stage 1 indicates that less CSH gel was formed in U-BF compared to U. However, the higher dehydration of CSH gel after 105°C in Stage 1 indicates that more CSH gel was formed in U-BF compared to U. In Stage 2 (350°C-450°C), the second peak was linked with the dehydration of chemically bound water in portlandite ($Ca(OH)_2$) [74, 75]. The higher peak for the decomposition of $Ca(OH)_2$ in Stage 2 showed the availability of more $Ca(OH)_2$ in U-BF than in U. The third peak in Stage 3 was linked to the decomposition of calcium carbonate ($CaCO_3$) [54, 75]. Similarly, the higher peak for the decomposition of $CaCO_3$ in Stage 3 (450°C-700°C) revealed more availability of $CaCO_3$ in U-BF than in U. The fourth peak in Stage 4 (700°C-1000°C) was due to the transformation of C-S-H into wollastonite ($CaSiO_3$) [67, 68] and higher for the U-BF than that of U. However, the peaks of U-BF were slightly shifted to a higher temperature compared to those of U, indicating a delay in the dehydration/decomposition of ettringite, C-S-H gel, $Ca(OH)_2$, $CaCO_3$, and $CaSiO_3$. This delay can be attributed to the addition of basalt fiber, which helps to reduce the rate of heat transfer in UHPC, thereby slowing down the dehydration and decomposition process of hydration products after exposure to high-temperatures. This, in turn, can help to preserve the existing hydration products and promote the formation of additional C-S-H gel, $Ca(OH)_2$, $CaCO_3$, and $CaSiO_3$ after exposure to high-temperatures. The TG mass loss curves at various stages are shown in (Fig 14(b)). In Stage 1, initially the mass loss at 105°C was higher for U (7.1%), while for U-BF the mass loss was 6.86%. However, the overall mass loss was higher in U-BF (12.1%) than in U (11.9%). In Stage 2, the mass loss was higher in U-BF (1.29%) compared to that in U (1.23%). Similarly, in Stage 3 and stage 4, the mass loss was also higher for U-BF than that of U. Overall, the DTG and TG analyses revealed that the addition of basalt fiber in UHPC

led to delayed dehydration and decomposition of various hydration products (ettringite, C-S-H gel, $Ca(OH)_2$, $CaCO_3$, and $CaSiO_3$ after exposure to high-temperatures.

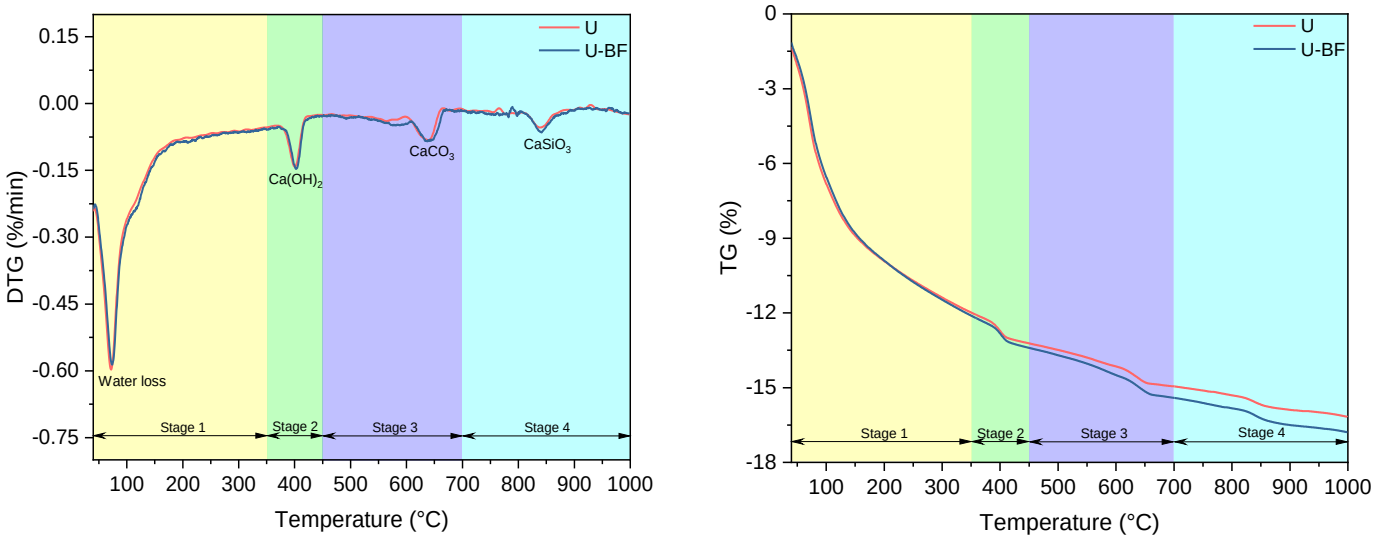

(a) Derivative thermogravimetry analysis (b) Thermogravimetry analysis

Fig 14. Thermal analysis of plain and basalt fiber reinforced UHPC

3.5.3. FTIR analysis to observe the changes in chemical structure of UHPC after exposure to high-temperature

Fig 15 (a)-(b) shows the FTIR spectra of plain and basalt fiber reinforced UHPC, illustrating the difference in hydration production at higher temperatures. In the FTIR spectra, the absorption band near 875 cm^{-1} and 1417 cm^{-1} represents the C-O bond in $CaCO_3$ [76]. The main absorption band near 966 cm^{-1} indicates the Si-O bond in the C-S-H gel [76]. The peak between 1060-1160 cm^{-1} in the FTIR spectra represents the Si-O in pure silica gel [76]. At ambient temperature, the quantity of C-S-H and silica gel is lower in U-BF compared to U (refer to Fig 16(b)). At 250°C, the C-S-H gel progressively increases in U-BF, showing more hydration of unreacted particles compared to U. At 500°C and 750°C, U-BF shows the formation of more $CaCO_3$ compared to U, indicating the formation of healing material in the cracks (due to dehydration and decomposition of C-S-H gel

and $Ca(OH)_2$) as evident from TG analysis in previous section. Also, the peak of C-S-H gel was shifted from 965 to 920 cm^{-1} (towards the peak of $CaCO_3$) showing the change in chemical structure of C-S-H gel due to depolymerization. This indicates that the C-S-H gel was decomposed at 750°C indicating the formation of $CaCO_3$. At 1000°C, the peak of Si-O bond in the C-S-H gel shifted from 965 to 900 cm^{-1} as shown in Fig 15(a)-(b), indicating changes in chemical structure of resulting hydration products, i.e., $CaSiO_3$ as evident from TG analysis in previous section. Therefore, the peak at 900 cm^{-1} in the FTIR spectra represents $CaSiO_3$, indicating the transformation of C-S-H gel. Meiszterics and Sinkó [77] also reported that the peak between 850 cm^{-1} to 1000 cm^{-1} is associated with the calcium metasilicate in $CaSiO_3$ at 1000°C.

Deconvolution analysis of the FTIR spectra was performed to quantify the $CaCO_3$ (Peak 1 and Peak 4), C-S-H gel (Peak 2), and silica gel (Peak 3) in plain and basalt fiber reinforced UHPC, as shown in Fig 16 (a). At ambient temperature, area of peak 2 (C-S-H gel) and peak 3 (silica gel) is lower in U-BF compared to U (refer to Fig 16(b)). This is inline with the results of hydration kinematics indicating the formation of less C-S-H gel during early stage as well as TG analysis indicating the less mass loss at AT. At 250°C, the area of peak 2 (C-S-H gel) progressively increased indicating the higher amount of C-S-H gel in U-BF as compared to that of U. This also supports the results of TG analysis indicating a higher amount of mass loss in U-BF. At 500°C and 750°C, the area of peak 2 (C-S-H gel) decreased while the area of peak 3 ($CaCO_3$) progressively increased. This indicates the formation of higher amount of $CaCO_3$ at this stage while the decrease in C-S-H gel was obvious due to its decomposition and depolymerization as this peak was shifted towards the lower wavelength. The formation of higher amount of $CaCO_3$ in U-BF is also evident from the results of TG analysis. At 1000°C, U-BF shows higher areas for peak 1 and peak 4 ($CaCO_3$) and peak 3 (silica gel) compared to U, while peak 2 ($CaSiO_3$) had lower area. Thus, the

addition of basalt fiber to UHPC leads to an increase in the formation of healing materials after exposure to high-temperatures. Therefore, the basalt fiber reinforcement can enhance the self-healing ability of UHPC at high-temperatures.

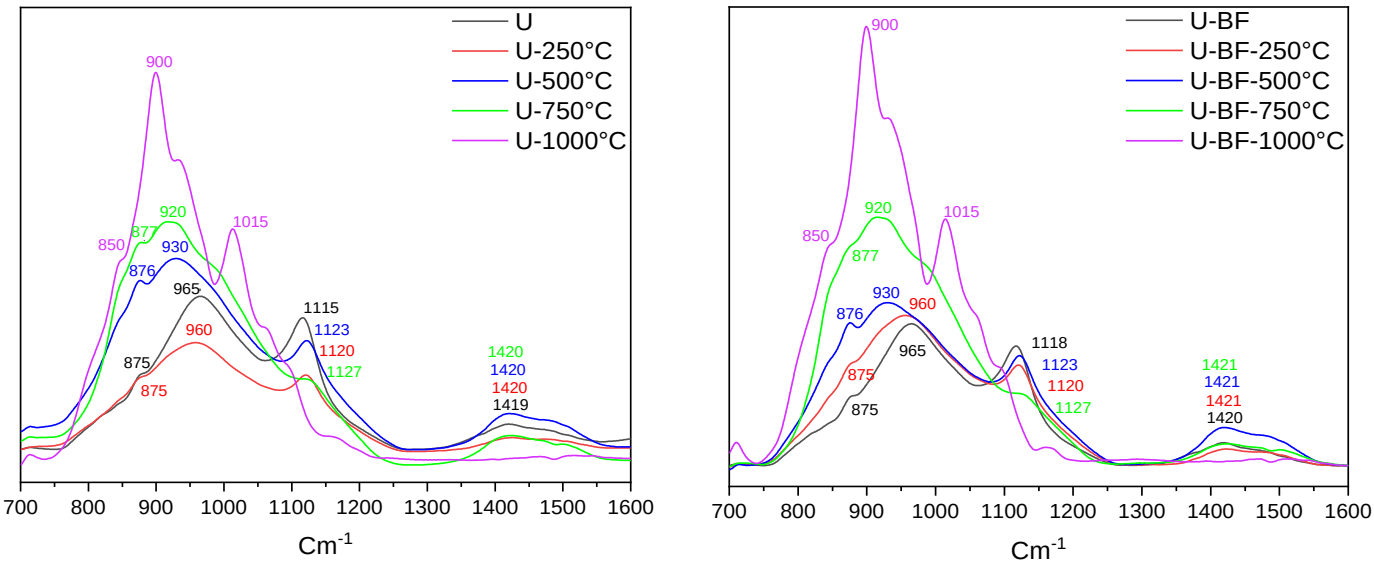

(a) Plain UHPC (b) Basalt fiber reinforced UHPC

Fig 15. FTIR analysis of plain and basalt fiber reinforced UHPC

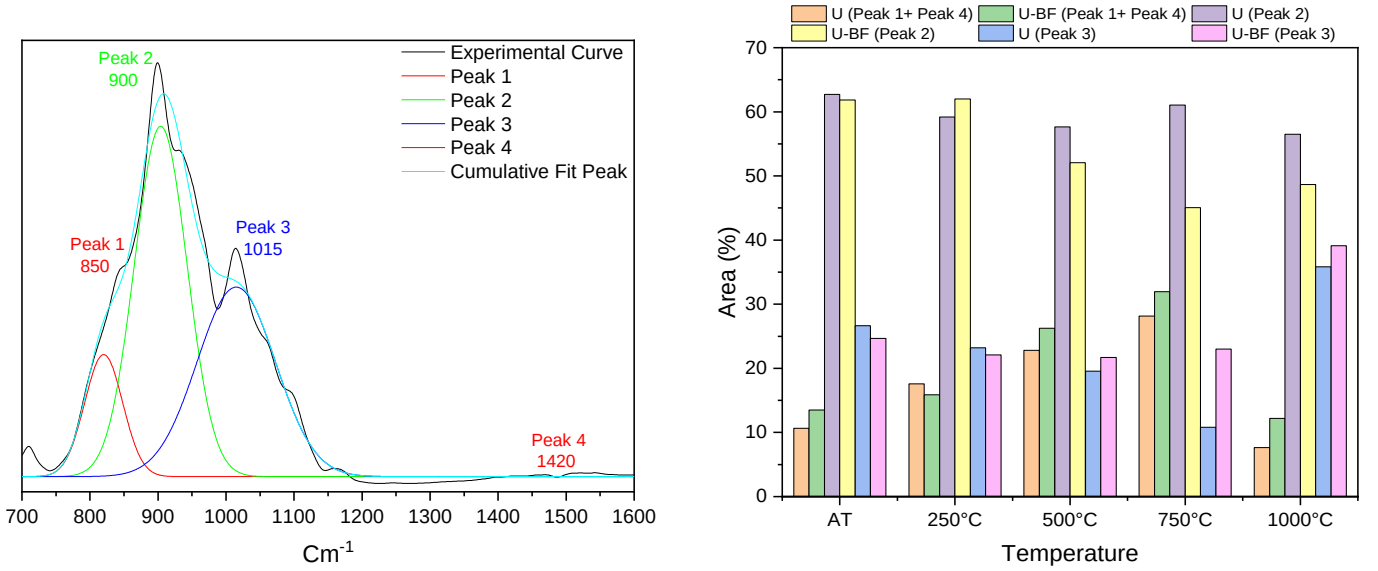

(a) Deconvoluted spectra (b) Area (%) of the deconvoluted components

Fig 16. FTIR deconvoluted analysis of plain and basalt fiber reinforced UHPC

4. Discussion

This study investigated the effect of hybrid steel and basalt fibers on the behavior of UHPC at high temperatures. Basalt fibers can help prevent explosive spalling in UHPC with their unique features and mechanisms. When exposed to high temperatures, basalt fibers offer several advantages for spalling prevention. Firstly, basalt fibers have a higher melting point than natural or polymer fibers. This allows them to remain stable and structurally intact even in high-temperatures environments, effectively reinforcing the UHPC and reducing the risk of spalling. Secondly, adding basalt fibers creates a reinforcing element network within the UHPC matrix. This fiber network serves as a secondary reinforcement system, distributing stresses and controlling crack propagation. Basalt fibers enhance resistance to crack development and propagation, thereby reducing the probability of spalling and improving the compressive characteristics of the UHPC. Additionally, when subjected to high temperatures, basalt fibers can generate voids or pores within the UHPC. These voids or pores serve as waterways for the release of vapor produced by the evaporation of water within the UHPC's inner structure. By allowing the escape of vapor pressure, the basalt fibers help alleviate internal pressure and prevent explosive spalling. Overall, the high melting point, reinforcing effect, and ability to create pores for vapor release make basalt fibers effective in preventing explosive spalling. This study’s findings hold significant potential for developing better UHPC with a hybrid of steel and basalt fibers that can withstand high-temperatures.

5. Conclusions

This study investigates the behavior of a hybrid steel-basalt fiber reinforced UHPC after exposure to high-temperatures and aims to provide insights into the efficacy of inorganic basalt fibers in preventing explosive spalling. The following conclusions can be drawn:

- Hybrid steel-basalt fiber reinforced UHPC (U-1.5ST+0.5BF) has superior spalling resistance and better integrity after exposure to high-temperatures compared to plain UHPC.
- The hybrid mix of 1.5% steel and 0.5% basalt fiber content in UHPC was suggested as an better mix after exposure to high-temperatures for residual compressive strength.
- The SEM images show that hybrid steel-basalt fiber reinforced UHPC exhibited better crack resistance and healing properties after exposure to high-temperatures compared to plain UHPC.
- The Micro XCT test revealed that hybrid steel-basalt fiber reinforced UHPC had higher porosity as compared to plain UHPC at ambient temperatures and porosity further increased after exposure to high-temperatures, which was crucial in providing the spalling resistance to UHPC.
- The calorimetry test shows that adding basalt fibers to UHPC improves early formation of CSH gel and $Ca(OH)_2$ during the acceleration period by maintaining a uniform water distribution but reduces heat flow and formation of CSH gel and $Ca(OH)_2$ during the deceleration period.
- Through the TG analysis, it was observed that the inclusion of basalt fibers in UHPC results in the retardation of dehydration and decomposition of different hydration products at high-temperatures.
- From the FTIR analysis, it has been observed that the incorporation of basalt fiber reinforcement in UHPC leads to a significant increase in the formation of healing materials after exposure to high-temperatures.

- The hybrid of steel-basalt fiber reinforced UHPC was found effective in preventing explosive spalling after exposure to high-temperature that led to ensure the safety of UHPC structures exposed to fire.

CRediT authorship contribution statement

Mehran Khan: Conceptualization, Methodology, Investigation, Formal analysis, Writing–original draft, Writing–review & editing. **Jiancong Lao:** Investigation, Data Curation, Resources, Validation. **Muhammad Riaz Ahmad:** Visualization, Methodology, Formal analysis, Software, Writing–review & editing. **Jian-Guo Dai:** Conceptualization, Methodology, Funding acquisition, Project administration, Writing–review & editing, Supervision.

Declaration of Competing Interest

The authors declare that they have no known competing financial interests or personal relationships that could have appeared to influence the work reported in this paper.

Acknowledgment

The financial support for the first authors from Research Grant Council of Hong Kong SAR (Project code: 15219919) and the Postdoc Matching Fund Scheme (Project codes: P0014094 and P0005306) at The Hong Kong Polytechnic University is gratefully acknowledged.

References:

[1] B.-T. Huang, J.-Q. Wu, J. Yu, J.-G. Dai, C.K. Leung, V.C. Li, Seawater sea-sand engineered/strain-hardening cementitious composites (ECC/SHCC): Assessment and modeling of crack characteristics, Cement and Concrete Research 140 (2021) 106292.
[2] J.-G. Dai, B.-T. Huang, S.P. Shah, Recent Advances in Strain-Hardening UHPC with Synthetic Fibers, Journal of Composites Science 5(10) (2021) 283.
[3] Q. Meng, C. Wu, J. Li, Z. Liu, P. Wu, Y. Yang, Z. Wang, Steel/basalt rebar reinforced Ultra-High Performance Concrete components against methane-air explosion loads, Composites Part B: Engineering 198 (2020) 108215.

[4] P. Li, M.J. Sluijsmans, H. Brouwers, Q. Yu, Functionally graded ultra-high performance cementitious composite with enhanced impact properties, Composites Part B: Engineering 183 (2020) 107680.
[5] T.C. 37-2018, Fundamental characteristics and test methods of ultra-high performance concrete, China Building Material Council: Beijing, China (2018).
[6] B.-T. Huang, Y.-T. Wang, J.-Q. Wu, J. Yu, J.-G. Dai, C.K. Leung, Effect of fiber content on mechanical performance and cracking characteristics of ultra-high-performance seawater sea-sand concrete (UHP-SSC), Advances in Structural Engineering 24(6) (2021) 1182-1195.
[7] F. Sciarretta, S. Fava, M. Francini, L. Ponticelli, M. Caciolai, B. Briseghella, C. Nuti, Ultra-High performance concrete (UHPC) with polypropylene (Pp) and steel Fibres: Investigation on the high temperature behaviour, Construction and Building Materials 304 (2021) 124608.
[8] Y. Li, P. Pimienta, N. Pinoteau, K.H. Tan, Effect of aggregate size and inclusion of polypropylene and steel fibers on explosive spalling and pore pressure in ultra-high-performance concrete (UHPC) at elevated temperature, Cement and Concrete Composites 99 (2019) 62-71.
[9] D. Zhang, A. Dasari, K.H. Tan, On the mechanism of prevention of explosive spalling in ultra-high performance concrete with polymer fibers, Cement and Concrete Research 113 (2018) 169-177.
[10] Y. Li, D. Zhang, Effect of lateral restraint and inclusion of polypropylene and steel fibers on spalling behavior, pore pressure, and thermal stress in ultra-high-performance concrete (UHPC) at elevated temperature, Construction and Building Materials 271 (2021) 121879.
[11] Y. Li, K.H. Tan, E.-H. Yang, Synergistic effects of hybrid polypropylene and steel fibers on explosive spalling prevention of ultra-high performance concrete at elevated temperature, Cement and Concrete Composites 96 (2019) 174-181.
[12] M. Ozawa, S.S. Parajuli, Y. Uchida, B. Zhou, Preventive effects of polypropylene and jute fibers on spalling of UHPC at high temperatures in combination with waste porous ceramic fine aggregate as an internal curing material, Construction and Building Materials 206 (2019) 219-225.
[13] M. Khan, J. Lao, M.R. Ahmad, M.-F. Kai, J.-G. Dai, The role of calcium aluminate cement in developing an efficient ultra-high performance concrete resistant to explosive spalling under high temperatures, Construction and Building Materials 384 (2023) 131469.
[14] G. Ren, X. Gao, H. Zhang, Utilization of hybrid sisal and steel fibers to improve elevated temperature resistance of ultra-high performance concrete, Cement and Concrete Composites 130 (2022) 104555.
[15] D. Zhang, Y. Liu, K.H. Tan, Spalling resistance and mechanical properties of strain-hardening ultra-high performance concrete at elevated temperature, Construction and Building Materials 266 (2021) 120961.
[16] G. Choe, G. Kim, N. Gucunski, S. Lee, Evaluation of the mechanical properties of 200 MPa ultra-high-strength concrete at elevated temperatures and residual strength of column, Construction and Building Materials 86 (2015) 159-168.
[17] J.-H. Lee, Y.-S. Sohn, S.-H. Lee, Fire resistance of hybrid fibre-reinforced, ultra-high-strength concrete columns with compressive strength from 120 to 200 MPa, Magazine of Concrete Research 64(6) (2012) 539-550.
[18] Y. Du, H.-H. Qi, S.-S. Huang, J.R. Liew, Experimental study on the spalling behaviour of ultra-high strength concrete in fire, Construction and Building Materials 258 (2020) 120334.

[19] D. Zhang, G.Y. Tan, K.H. Tan, Combined effect of flax fibers and steel fibers on spalling resistance of ultra-high performance concrete at high temperature, Cement and Concrete Composites 121 (2021) 104067.
[20] M.R. Bangi, T. Horiguchi, Pore pressure development in hybrid fibre-reinforced high strength concrete at elevated temperatures, Cement and Concrete Research 41(11) (2011) 1150-1156.
[21] V. Kodur, F.-P. Cheng, T.-C. Wang, M. Sultan, Effect of strength and fiber reinforcement on fire resistance of high-strength concrete columns, Journal of Structural Engineering 129(2) (2003) 253-259.
[22] D. Zhang, K.H. Tan, A. Dasari, Y. Weng, Effect of natural fibers on thermal spalling resistance of ultra-high performance concrete, Cement and Concrete Composites 109 (2020) 103512.
[23] M. Ozawa, Z. Bo, J. Kawaguchi, Y. Uchida, Preventive effect on spalling of UFC using jute fiber at high temperature, MATEC web of conferences, EDP Sciences, 2013, p. 02006.
[24] J. Xu, A. Kang, Z. Wu, P. Xiao, Y. Gong, Effect of high-calcium basalt fiber on the workability, mechanical properties and microstructure of slag-fly ash geopolymer grouting material, Construction and Building Materials 302 (2021) 124089.
[25] W.-Y. Gao, K.-X. Hu, J.-G. Dai, K. Dong, K.-Q. Yu, L.-J. Fang, Repair of fire-damaged RC slabs with basalt fabric-reinforced shotcrete, Construction and Building Materials 185 (2018) 79-92.
[26] M. Khan, M. Cao, A. Hussain, S. Chu, Effect of silica-fume content on performance of CaCO3 whisker and basalt fiber at matrix interface in cement-based composites, Construction and Building Materials 300 (2021) 124046.
[27] M. Khan, M. Cao, Effect of hybrid basalt fibre length and content on properties of cementitious composites, Magazine of Concrete Research 73(10) (2021) 487-498.
[28] M. Khan, M. Cao, X. Chaopeng, M. Ali, Experimental and analytical study of hybrid fiber reinforced concrete prepared with basalt fiber under high temperature, Fire and Materials (2021).
[29] R. Ralegaonkar, H. Gavali, P. Aswath, S. Abolmaali, Application of chopped basalt fibers in reinforced mortar: A review, Construction and Building Materials 164 (2018) 589-602.
[30] M. Farouk, A. Soltan, S. Schlüter, E. Hamzawy, A. Farrag, A. El-Kammar, A. Yahya, H. Pollmann, Optimization of microstructure of basalt-based fibers intended for improved thermal and acoustic insulations, Journal of Building Engineering 34 (2021) 101904.
[31] F. Şahin, M. Uysal, O. Canpolat, Y. Aygörmez, T. Cosgun, H. Dehghanpour, Effect of basalt fiber on metakaolin-based geopolymer mortars containing rilem, basalt and recycled waste concrete aggregates, Construction and Building Materials 301 (2021) 124113.
[32] M. Khan, M. Cao, M. Ali, Cracking behaviour and constitutive modelling of hybrid fibre reinforced concrete, Journal of Building Engineering 30 (2020) 101272.
[33] M. Khan, M. Cao, M. Ali, Effect of basalt fibers on mechanical properties of calcium carbonate whisker-steel fiber reinforced concrete, Construction and Building Materials 192 (2018) 742-753.
[34] H. Jamshaid, R. Mishra, A green material from rock: basalt fiber–a review, The Journal of The Textile Institute 107(7) (2016) 923-937.
[35] A.M. Jabbar, M.J. Hamood, D.H. Mohammed, The effect of using basalt fibers compared to steel fibers on the shear behavior of ultra-high performance concrete T-beam, Case Studies in Construction Materials 15 (2021) e00702.

[36] S.-T. Kang, J.-I. Choi, K.-T. Koh, K.S. Lee, B.Y. Lee, Hybrid effects of steel fiber and microfiber on the tensile behavior of ultra-high performance concrete, Composite Structures 145 (2016) 37-42.
[37] J. Gong, Y. Ma, J. Fu, J. Hu, X. Ouyang, Z. Zhang, H. Wang, Utilization of fibers in ultra-high performance concrete: A review, Composites Part B: Engineering (2022) 109995.
[38] A. Committee, ASTM C618-19 Standard specification for coal fly ash and raw or calcined natural pozzolan for use in concrete, Barr Harbor Drive, West Conshohocken: Annual Book of ASTM Standards (2019).
[39] J. Yang, G.-F. Peng, J. Zhao, G.-S. Shui, On the explosive spalling behavior of ultra-high performance concrete with and without coarse aggregate exposed to high temperature, Construction and Building Materials 226 (2019) 932-944.
[40] S. Banerji, V. Kodur, Effect of temperature on mechanical properties of ultra‐high performance concrete, Fire and Materials (2021).
[41] S. Sanchayan, S.J. Foster, High temperature behaviour of hybrid steel–PVA fibre reinforced reactive powder concrete, Materials and Structures 49 (2016) 769-782.
[42] X. Liang, C. Wu, Y. Yang, Z. Li, Experimental study on ultra-high performance concrete with high fire resistance under simultaneous effect of elevated temperature and impact loading, Cement and Concrete Composites 98 (2019) 29-38.
[43] X. Liang, C. Wu, Y. Su, Z. Chen, Z. Li, Development of ultra-high performance concrete with high fire resistance, Construction and Building Materials 179 (2018) 400-412.
[44] V. Kodur, S. Banerji, R. Solhmirzaei, Effect of temperature on thermal properties of ultrahigh-performance concrete, Journal of Materials in Civil Engineering 32(8) (2020) 04020210.
[45] K. Liu, J. Liu, J. Li, M. Tao, C. Wu, Experimental investigation of heating–cooling effects on the mechanical properties of geopolymer-based high performance concrete heated to elevated temperatures, Structures, Elsevier, 2023, pp. 735-747.
[46] K. Liu, C. Wu, X. Li, J. Liu, M. Tao, J. Fang, S. Xu, The influences of cooling regimes on fire resistance of ultra-high performance concrete under static-dynamic coupled loads, Journal of Building Engineering 44 (2021) 103336.
[47] K. Liu, C. Wu, X. Li, M. Tao, J. Li, J. Liu, S. Xu, Fire damaged ultra-high performance concrete (UHPC) under coupled axial static and impact loading, Cement and Concrete Composites 126 (2022) 104340.
[48] M. Kabir, H. Wang, K. Lau, F. Cardona, Effects of chemical treatments on hemp fibre structure, Applied Surface Science 276 (2013) 13-23.
[49] X. Xiong, M. Wu, W. Shen, J. Li, D. Zhao, P. Li, J. Wu, Performance and microstructure of ultra-high-performance concrete (UHPC) with silica fume replaced by inert mineral powders, Construction and Building Materials 327 (2022) 126996.
[50] S.-H. Kang, J.-H. Lee, S.-G. Hong, J. Moon, Microstructural investigation of heat-treated ultra-high performance concrete for optimum production, Materials 10(9) (2017) 1106.
[51] A. C109/C109M-16a, Standard test method for compressive strength of hydraulic cement mortars (Using 2-in. or [50-mm] cube specimens), West Conshohocken: ASTM International (2016).
[52] B. Chen, J. Liu, Residual strength of hybrid-fiber-reinforced high-strength concrete after exposure to high temperatures, Cement and Concrete Research 34(6) (2004) 1065-1069.
[53] W. Zheng, B. Luo, Y. Wang, Microstructure and mechanical properties of RPC containing PP fibres at elevated temperatures, Magazine of Concrete Research 66(8) (2014) 397-408.

[54] G.-F. Peng, X.-J. Niu, Y.-J. Shang, D.-P. Zhang, X.-W. Chen, H. Ding, Combined curing as a novel approach to improve resistance of ultra-high performance concrete to explosive spalling under high temperature and its mechanical properties, Cement and Concrete Research 109 (2018) 147-158.
[55] K. Cao, G. Liu, H. Li, Z. Huang, Mechanical properties and microstructures of Steel-basalt hybrid fibers reinforced Cement-based composites exposed to high temperatures, Construction and Building Materials 341 (2022) 127730.
[56] A. Alaskar, A. Albidah, A.S. Alqarni, R. Alyousef, H. Mohammadhosseini, Performance evaluation of high-strength concrete reinforced with basalt fibers exposed to elevated temperatures, Journal of Building Engineering 35 (2021) 102108.
[57] Y. Zhu, H. Hussein, A. Kumar, G. Chen, A review: Material and structural properties of UHPC at elevated temperatures or fire conditions, Cement and Concrete Composites 123 (2021) 104212.
[58] H. Huang, R. Wang, X. Gao, Improvement effect of fiber alignment on resistance to elevated temperature of ultra-high performance concrete, Composites Part B: Engineering 177 (2019) 107454.
[59] R. Way, K. Wille, Effect of heat-induced chemical degradation on the residual mechanical properties of ultrahigh-performance fiber-reinforced concrete, Journal of Materials in Civil Engineering 28(4) (2016) 04015164.
[60] N. Lee, K. Koh, S. Park, G. Ryu, Microstructural investigation of calcium aluminate cement-based ultra-high performance concrete (UHPC) exposed to high temperatures, Cement and Concrete Research 102 (2017) 109-118.
[61] Q. Zhang, G. Ye, E. Koenders, Investigation of the structure of heated Portland cement paste by using various techniques, Construction and Building Materials 38 (2013) 1040-1050.
[62] M. Amran, A.M. Onaizi, D.N. Qader, G. Murali, Innovative use of fly ash-finely powdered glass cullet as a nano additives for a sustainable concrete: Strength and microstructure and cost analysis, Case Studies in Construction Materials 17 (2022) e01688.
[63] H.-W. Reinhardt, M. Jooss, Permeability and self-healing of cracked concrete as a function of temperature and crack width, Cement and concrete research 33(7) (2003) 981-985.
[64] Q. Zheng, C. Li, F. Song, B. He, W. Li, Z. Jiang, Autogenous self-healing of ultra-high-performance fiber-reinforced concrete with varying silica fume dosages: Secondary hydration and structural regeneration, Cement and Concrete Composites 137 (2023) 104905.
[65] S. Hou, K. Li, Z. Wu, F. Li, C. Shi, Quantitative evaluation on self-healing capacity of cracked concrete by water permeability test–A review, Cement and Concrete Composites 127 (2022) 104404.
[66] A. Beglarigale, D. Eyice, B. Tutkun, H. Yazıcı, Evaluation of enhanced autogenous self-healing ability of UHPC mixtures, Construction and Building Materials 280 (2021) 122524.
[67] J.-X. Lu, P. Shen, Y. Sun, C.S. Poon, Strategy for preventing explosive spalling and enhancing material efficiency of lightweight ultra high-performance concrete, Cement and Concrete Research 158 (2022) 106842.
[68] E.T. Rodriguez, K. Garbev, D. Merz, L. Black, I.G. Richardson, Thermal stability of CSH phases and applicability of Richardson and Groves' and Richardson C-(A)-SH (I) models to synthetic CSH, Cement and Concrete research 93 (2017) 45-56.
[69] X. Hu, J. Xiao, Z. Zhang, C. Wang, C. Long, L. Dai, Effects of CCCW on properties of cement-based materials: A review, Journal of Building Engineering 50 (2022) 104184.

[70] J.-I. Choi, B.Y. Lee, Bonding properties of basalt fiber and strength reduction according to fiber orientation, Materials 8(10) (2015) 6719-6727.
[71] Y. Shi, G. Long, C. Ma, Y. Xie, J. He, Design and preparation of ultra-high performance concrete with low environmental impact, Journal of Cleaner Production 214 (2019) 633-643.
[72] J. Wei, S. Ma, G.T. D'Shawn, Correlation between hydration of cement and durability of natural fiber-reinforced cement composites, Corrosion Science 106 (2016) 1-15.
[73] G. Delannoy, S. Marceau, P. Gle, E. Gourlay, M. Guéguen-Minerbe, D. Diafi, S. Amziane, F. Farcas, Impact of hemp shiv extractives on hydration of Portland cement, Construction and Building Materials 244 (2020) 118300.
[74] P. Shen, J.-X. Lu, L. Lu, Y. He, F. Wang, S. Hu, An alternative method for performance improvement of ultra-high performance concrete by internal curing: Role of physicochemical properties of saturated lightweight fine aggregate, Construction and Building Materials 312 (2021) 125373.
[75] D. Suescum-Morales, J.D. Ríos, A. Martínez-De La Concha, H. Cifuentes, J.R. Jiménez, J.M. Fernández, Effect of moderate temperatures on compressive strength of ultra-high-performance concrete: A microstructural analysis, Cement and Concrete Research 140 (2021) 106303.
[76] I.G. Lodeiro, D.E. Macphee, A. Palomo, A. Fernández-Jiménez, Effect of alkalis on fresh C–S–H gels. FTIR analysis, Cement and Concrete Research 39(3) (2009) 147-153.
[77] A. Meiszterics, K. Sinkó, Sol–gel derived calcium silicate ceramics, Colloids and Surfaces A: Physicochemical and Engineering Aspects 319(1-3) (2008) 143-148.